Boletín de la Sociedad Española de Cerámica y Vidrio
Vol 53, 1, 21-26, Enero-Febrero 2014 ISSN 0366-3175. eISSN 2173-0431.
doi: 10.3989/cyv.32014

BOLETIN DE LA SOCIEDAD ESPAÑOLA DE
Cerámica y Vidrio
A R T I C U L O

Evolution of the crystalline structure in $(Bi_{0.5}Na_{0.5})_{1-x}Ba_xTiO_3$ thin films around the Morphotropic Phase Boundary

D. PÉREZ-MEZCUA[1,2], M. L. CALZADA[1], I. BRETOS[1], J. RICOTE[1], D. CHATEIGNER[3], R. ESCOBAR-GALINDO[1], R. JIMENEZ[1] AND R. SIRERA[2]

[1]Consejo Superior de Investigaciones Científicas (CSIC), Instituto de Ciencia de Materiales de Madrid (ICMM), Madrid, Spain, 28049
[2]Departamento de Química y Edafología, Facultad de Ciencias, Universidad de Navarra, Navarra, Spain, 31008
[3]Université de Caen Basse-Normandie, Laboratoire de Cristallographie et Sciences des Matériaux (CRISMAT), Caen, France, 14050

$(Bi_{0.5}Na_{0.5})_{1-x}Ba_xTiO_3$ (BNBT), which exhibits compositions for the morphotropic phase boundary (MPB) where exist an intimate coexistence of the rhombohedral and tetragonal structures, is being considered as promising lead-free alternative to the well known $Pb(Zr_xTi_{1-x})O_3$ (PZT). In this work, BNBT thin films were fabricated by chemical solution deposition (CSD) with a wide range of compositions (x~0.050-0.150) onto $Pt/TiO_2/SiO_2/(100)Si$ substrates. Structural studies by X-ray diffraction (λ_{Cu}~1.5406 Å) using a four-circle goniometer were carried out to determine the crystalline structure of the films. Rietveld analysis of the experimental X-ray patterns showed different volume fractions of the rhombohedral and tetragonal phases as a function of the Ba^{2+} content and the coexistence of both phases, characteristic of a MPB region, for x~0.055-0.080. Finally, Rutherford backscattering experiments (RBS) were performed to determine the compositional profile of the films. This study revealed a homogenous composition of the BNBT films with abrupt film/substrate interfaces.

Keywords: Thin films, lead-free ferroelectrics, morphotropic phase boundary.

Evolución de la estructura cristalina en láminas delgadas de $(Bi_{0.5}Na_{0.5})_{1-x}Ba_xTiO_3$ próximas a la Frontera de Fase Morfotrópica

El $(Bi_{0.5}Na_{0.5})_{1-x}Ba_xTiO_3$ (BNBT), considerado un posible candidato sin plomo para substituir al $Pb(Zr_xTi_{1-x})O_3$ (PZT), presenta una frontera de fase morfotrópica donde se da la coexistencia de las estructuras tetragonal y romboédrica. En este trabajo, se han fabricado láminas delgadas de BNBT por depósito químico de disoluciones (CSD) con composiciones comprendidas entre x~ 0.050 y x~ 0.150 sobre substratos de $Pt/TiO_2/SiO_2/(100)Si$. En dichas láminas se ha llevado a cabo un estudio estructural empleando difracción de rayos X (DRX) (λ_{Cu}~1.5406 Å) y un goniómetro de cuatro círculos. El análisis Rietveld de los patrones experimentales de DRX mostró: i) diferentes fracciones volumétricas para las fases romboédrica y tetragonal, en función del contenido de Ba^{2+} ii) la coexistencia de ambas estructuras, característico de una región MPB, para composiciones con x~0.055-0.080. Finalmente, se determinó el perfil composicional de las láminas de BNBT por espectroscopía de retrodispersión Rutherford (RBS). Este estudio demostró que las láminas de BNBT presentan una composición homogénea e intercaras abruptas lámina/substrato.

Palabras clave: Láminas delgadas, ferroeléctricos sin plomo, frontera de fase morfotrópica.

1. INTRODUCTION

Lead-Zirconium-Titanium oxide $Pb(Zr_xTi_{1-x})O_3$ (PZT), a solid solution of ferroelectric $PbTiO_3$ and antiferroelectric $PbZrO_3$ (1), has drawn considerable interest for memories, actuators, sensors and transductors. An enhancement of dielectric, ferroelectric and piezoelectric properties has been reported for compositions close to the morphotropic phase boundary (MPB) (2) where the coexistence of two ferroelectric phases leads to a large number of polarization directions related to crystallographic orientations, resulting in anomalously high piezoelectric properties. Nevertheless, European directives have put restriction on the use of hazardous substances such as lead, for electronic components. Therefore, there is a high interest in substituting the most used ferro-piezoelectric material, the PZT, by lead-free ferro-piezoelectric compounds (3).

Bismuth sodium titanate $(Bi_{0.5}Na_{0.5})TiO_3$ (BNT) (4) is considered an excellent candidate as a key material of lead-free piezoelectric ceramics. BNT presents a perovskite structure with rhombohedral symmetry at room temperature, a phase transition from rhombohedral to tetragonal between 528-673 K and from tetragonal to cubic above 813 K (5).

BNT exhibits a strong ferroelectric response (Pr~38 $\mu C/cm^2$). However, it is difficult to obtain poled bulk ceramics due to the large coercive field (Ec~76 kV/cm). To facilitate the poling process, different solid solutions of BNT with other perovskites, such as binary systems containing $Bi_{0.5}K_{0.5}TiO_3$ (6), $BiFeO_3$ (7), $BaTiO_3$(8), or ternary systems like $Bi_{1/2}Na_{1/2}TiO_3$–$BaTiO_3$– $Bi_{1/2}K_{1/2}TiO_3$ (9) or $Bi_{1/2}Na_{1/2}TiO_3$–$Bi_{1/2}K_{1/2}TiO_3$ –$BiFeO_3$ (10), have been studied.

Among these solid solutions, mixtures of bismuth sodium titanate ($Bi_{1/2}$ $Na_{1/2}$)TiO_3 (BNT) and barium titanate $BaTiO_3$ (BT) in the MPB region $(Bi_{0.5}Na_{0.5})_{1-x}Ba_xTiO_3$ – (BNBT) are being studied in deep. A significant controversy related to the MPB region for the BNBT composition is found in the literature (11-14). Recent works, based on the variation of the electrical properties and in-situ synchrotron diffraction analysis, have positioned the MPB region for BNBT bulk ceramics for x values between 0.050 and 0.110, where the transition from the space group R3m to the P4mm one occurs (15).

Ferroelectric materials are of high interest for integrating with MEMSs (Microelectromechanical systems) because of their high piezoelectric response (16-17). For these applications, the ferroelectric has to be prepared in thin film form onto substrates. However, properties of the thin film differ from those of bulk ceramics, which is mainly associated to small grain size, development of microstrains or variations in the compositional depth profile. This can produce a shift in the MPB region in the film compared with bulk ceramics and a decrease in the properties (17-19).

In this work, the MPB region of solution derived lead-free $(Bi_{0.5}Na_{0.5})_{1-x}Ba_xTiO_3$ (BNBT) films is determined by X-ray diffraction. The compositional depth profiles obtained by Rutherford backscattering spectroscopy (RBS) and the micrographs from scanning electron microscopy of the MPB BNBT films have been also studied, inferring from these the optimum conditions to obtain thin films with appropriate functionalities.

2. EXPERIMENTAL PROCEDURE

2.1. Solutions, powders and thin films

A precursor sol of $(Bi_{0.5}Na_{0.5})TiO_3$ (BNT), and a precursor solution of $BaTiO_3$ (BT) were prepared following a solution method reported elsewhere (20-22). BNT sol and BT solution were mixed in order to obtain $(Bi_{0.50}Na_{0.50})_{1-x}Ba_xTiO_3$ solutions (BNBT) with the stoichiometric nominal compositions and with different content of Ba^{2+} (x~0.035, 0.055, 0.080 y 0.100). Hereafter, the resulting precursor solutions will be denoted BNBT3.5, BNBT5.5, BNBT8.0 and BNBT10.0.

The solutions were dried at 393 K for 72h and the resulting amorphous powders were annealed at 1173 K for 1h in air with a low heating and cooling rates, thus obtaining crystalline powders.

Diluted BNBT solutions (~0.2 mol/L) in ethanol (C_2H_6O, Sigma- Aldrich, 99.4 %) were deposited onto $Pt/TiO_2/SiO_2/(100)Si$ substrates (Radiant Technologies) by spin coating at 2000 rpm for 45 s and dried at 623 K for 60 s, in a hot plate. The gel layers were crystallized by rapid thermal processing (RTP, JetStar 100T JIPELEC) in an oxygen atmosphere at 923 K for 60 s (heating rate of ~303K·s^{-1}). Six layers of the diluted solutionwere successively deposited, dried and crystallized to obtain thin films with a thickness of ~300 nm. Films are referred to with the same names than the corresponding precursor solution.

2.2. Characterization of the crystalline powders and thin films

The crystalline phases developed in the BNBT powders with the different amounts of Ba^{2+} were monitored by X-Ray Diffraction (XRD). A Bruker D8 Advance and a Siemens D500 powder diffractometers with a Cu anode (λ~1.5406 Å) were used to carry out the measurements. The Siemens equipment had installed a k_β filter.

Diffraction patterns of the powders were measured in the 2θ interval between 20º and 60º, with a step of 0.05º per each 3s. More detailed patterns were recorded in the 2θ intervals between 39.0-41.0º and 46.0-47.5º, using a step of 0.005º per each 5s. (111) and (002)/(200) tetragonal reflections, and ($\bar{1}$11)/(111) and (200) rhombohedral reflections were collected in these intervals. The experimental patterns were analyzed with the V1-40 program, fitting the peaks to pseudo-Voigt functions (23).

Thin films were measured using an X-ray four-circle diffractometer (Huber) equipped with a position-sensitive detector (Model CPS-120, Inel, Inc). Complete XRD patterns of 120º in θ–2θ were obtained for each positions using a tilt angle from χ=0º to 55º, azimuthal angle from ϕ=0 to 355º and a regular grid of 5x5º.

Calculations were performed with the Materials Analysis Using Diffraction package (MAUD), in which not only the reflections of the perovskite structure (rhombohedral/tetragonal) but also from the Pt(111) top layer of the substrate were included for the Rietveld refinement. This makes possible to determine the cell size and volume fraction of the phases ascribed to the reflections coming from the perosvkite film and the contribution of the Pt(111) based on the layered method implemented in the software (24).

To obtain a detailed compositional depth profile of the films, Rutherford backscattering spectra (RBS) were collected with the 5 MeV HVEE Tandetron accelerator sited in the Centro de Microanalisis de Materiales de Madrid (CMAM). The RBS experiments were carried out using 2 MeV He^+ ions and a silicon surface barrier detector located at a scattering angle of 170º. The energy resolution of the detector is 16 keV for an ion dose of 10 μC. The experimental spectra were fitted with the software programs RBX (25) and SIMRA (26).

Micrographs (cross-section and plane view) of the thin films were obtained from a Field Emission Gun Scanning Electron Microscopy (FEG-SEM, Nova Nanosem 230).

3. RESULTS AND DISCUSSION

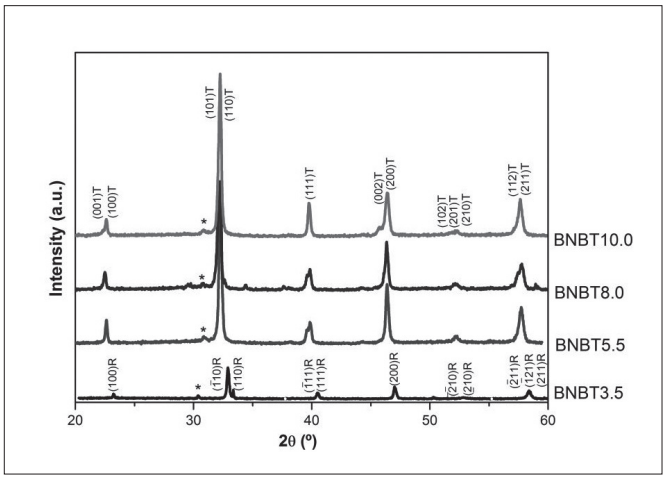

Figure 1. XRD patterns of powders using different BNT/BT molar ratios and recorded in the 2θ range of 20.0- 60.0º. * are ascribed to secondary phases.

Bol. Soc. Esp. Ceram. Vidr. Vol 53. 1, 21-26, Enero-Febrero 2014. ISSN 0366-3175. eISSN 2173-0431. doi: 10.3989/cyv.32014

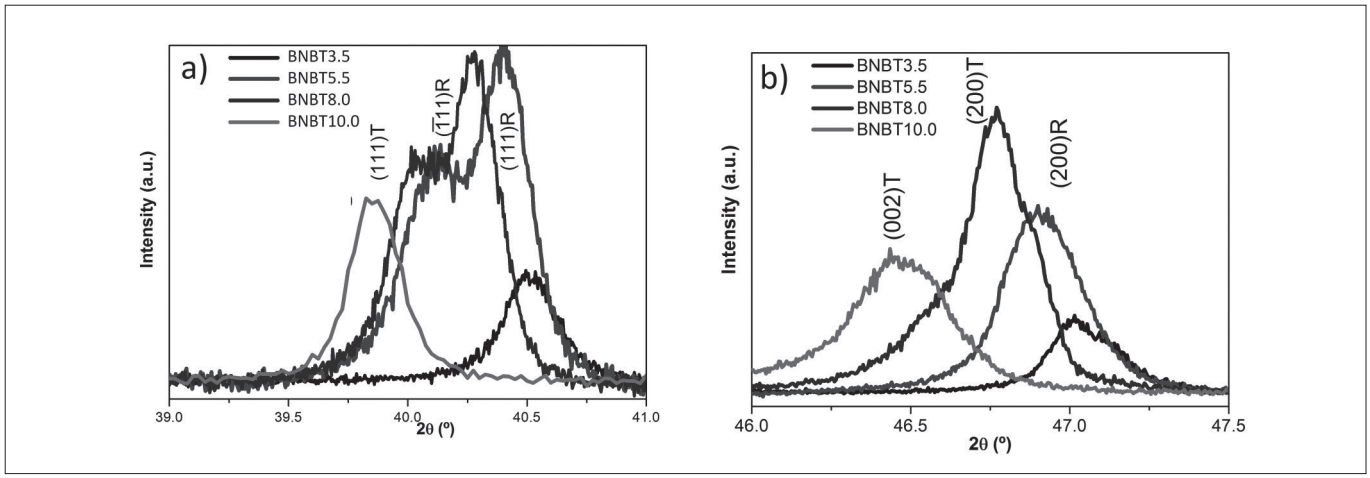

Figure 2. XRD patterns in the 2θ interval of a) 39.0º - 41.0º and b) 46.0º - 47.5º, which show the evolution from rhombohedral to tetragonal symmetry as a function of the Ba^{2+} content.

Figure 1 shows the XRD experimental patterns between 2θ values of 20.0º and 60.0º of the crystalline powders derived from the BNBT solutions. A perovskite structure is observed for the powders with the detection of a minor secondary phase, identified as close to the $Bi_2Ti_2O_7$ Fd$\bar{3}$m (JCPDS 32-118). R3m rhombohedral space group, described considering the rhombohedral axes, and P4mm tetragonal space group have been used to index the recorded patterns of the powders, according to the recent structural studies published for BNBT bulk ceramic (23).

The perovskite diffraction peak profiles, between 2θ values of 39.0º-41.0º and 46.0º-47.5º, for the BNBT powders as a function of the composition of the solid solution have been analyzed (Figure 2). The peaks shift towards lower 2θ angles with increasing the barium content. The reason is the larger size of the Ba^{2+} compared to the Bi^{3+} and Na^{+}; therefore,

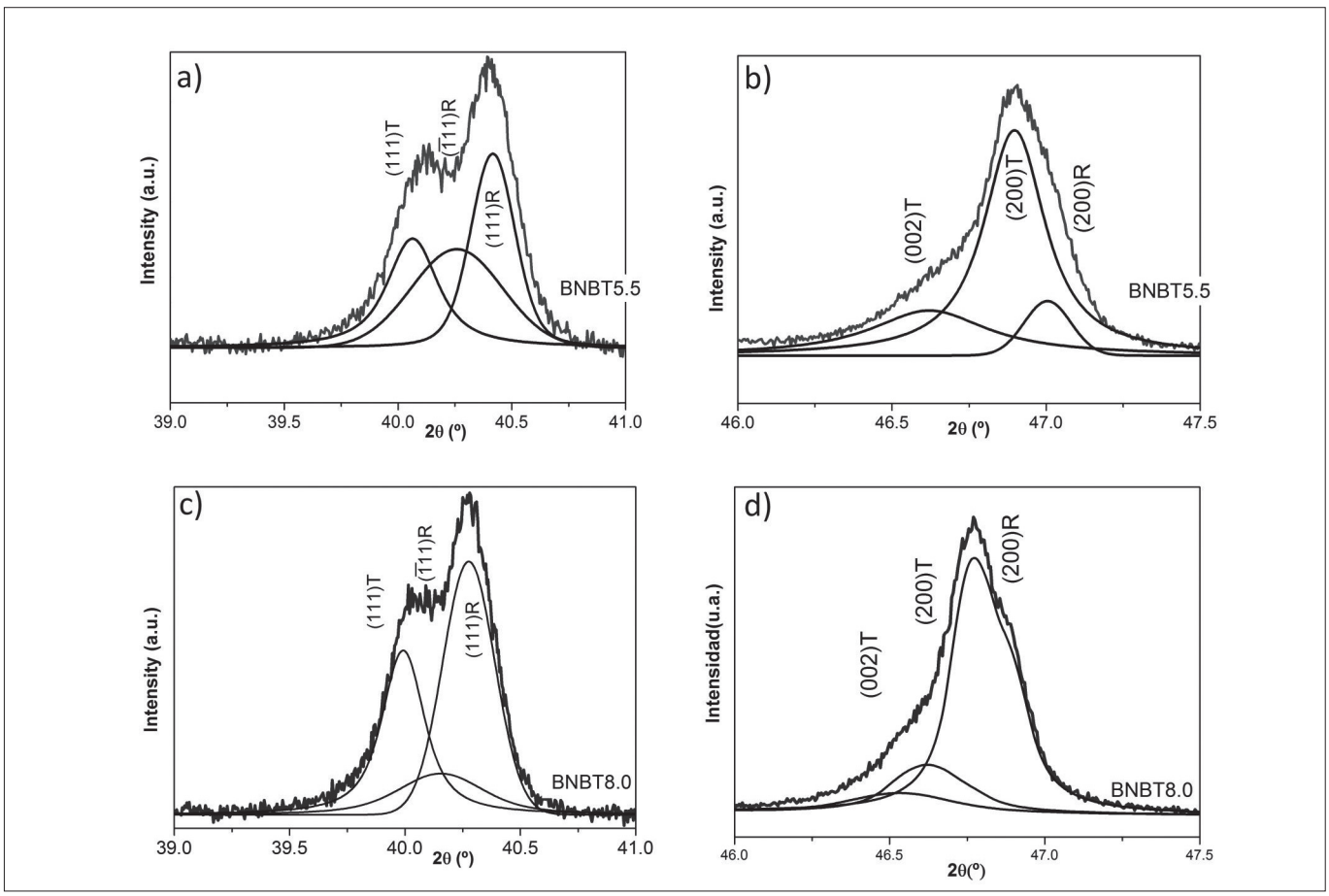

Figure 3. The deconvolution using Pseudo-Voight 2 functions of the X-ray recorded peaks corresponding to the BNBT 5.5 powders in the 2θ intervals of a) 39.0-41.0º (reliability ~4.9 %) b) 46.0-47.5º (reliability ~2.8 %). For the BNBT 8.0 powders the experimental and fitted peaks are shown in the 2θ ranges of c) 39.0-41.0º (reliability ~4.0 %) d) 46.0-47.5º (reliability ~4.9 %) corresponding to the BNBT8.0 powders. Both show the coexistence of the rhombohedral and tetragonal structures.

the interplanar spacing of the unit cell become larger as the content of Ba^{2+} increases.

The ($\bar{1}$11)/(111) and (200) reflections of the rhombohedral (R) phase at values of 2θ ~40.5º and ~47.0º, respectively, are recorded for the BNBT3.5 (Figure 2). On the contrary, the (111) and (002)/(200) reflections corresponding to the tetragonal (T) phase appear for the BNBT10.0 powders at ~40.0º and ~46.5º (Figure 2). The larger broadening of the peaks at 2θ values ~46.5º than that of the peaks of the BNBT3.5 powders could be explained by tetragonality ascribed to the splitting of the (002)/(200) reflections presented for samples with a large BT content (above x~0.080).

The shoulder observed between 2θ values of 39.0º-41.0º and 46.0º-47.5º for the BNBT5.5 and BNBT8.0 powders can indicate a coexistence of rhombohedral and tetragonal structures in these powders. These experimental peaks were modeled using a PseudoVoight-2 function (Figure 3). The peaks between 2θ~ 39.0-41.0º were well fitted to the (111)T and ($\bar{1}$11)/(111)R reflections (Figures 3a and 3c), whereas those between 2θ~ 46.0-47.5º were fitted to the (002)/(200)T and (200)R reflections (Figures 3b and 3d).

Unlike the XRD analysis of the powders, the microstrains and small grain size developed in thin films during the crystallization do not make possible their appropriate structural study using a conventional diffractometer. Both produce a large broadening of the XRD peaks of the films. In addition, some peaks from the substrate appear overlapped to those of the crystalline films. For the former reasons, structure analysis of the films is carried out using a four-circle diffractometer. The experimental XRD patterns have been fitted using the MAUD software (24) in order to determine the crystalline structure associated with the BNBT perovskite films and the Pt-bottom electrode layer of the substrate.

Figures 4 and 5 show the experimental and calculated profiles for the BNBT5.5 and BNBT8.0 films, respectively. Note the characteristic reflections of the perovskite observed for both films, without the detection of the second phases observed for the corresponding powders. In addition to the explained difficulties in the structural analysis of thin films, these samples present coexistence of rhombohedral (R3m)/tetragonal (P4mm) crystalline phases. Therefore, data acquisition of full diagrams for each (χ,ϕ) position was necessary using the four-circle diffractometer. From this study, it is observed that the MPB region is situated at x~0.055-0.080. Unlike the results reported for other authors for BNBT thin films (17-19), the MPB region here determined for films is located close to that reported for bulk ceramics and also to that obtained here for the corresponding powders (15, 23). The Rietveld refinement carried out on the experimental patterns of Figure 4 and 5 reveals the volume phase in the films of the rhombohedral and tetragonal structures. The refinement performance on BNBT5.5 and BNBT 8.0 films shows not only the coexistence of rhombohedral and tetragonal structures already observed in the corresponding powders (figure 3), but also the development of different crystalline structures, as demonstrated by the calculation of the volume fraction of the rhombohedral/ tetragonal phases for the BNBT 5.5 and BNBT 8.0 thin films. In the case of the BNBT5.5 film a large volume phase is obtained for the rhombohedral cell (~70 %) whereas the refinement of the XRD patterns for BNBT8.0 showed a volume fraction for the rhombohedral structure around ~33 %. On the contrary, the BNBT3.5 film is well fitted to a single rhombohedral phase, whereas that of the BNBT10.0 film fits to a single tetragonal structure.

Note that the crystallization of the films is carried out at 923K by a rapid thermal process (heating rate of ~30 $K{\cdot}s^{-1}$), whereas a conventional annealing at 1173K (heating rate of ~10 $K{\cdot}min^{-1}$) is used to obtain the crystalline powders. The differences in the thermal treatments used for the preparation of the films and the powders, and the extrinsic effect related to the special configuration of the thin film form, where a BNBT layer is supported onto a substrate, determine the variations in the crystalline structures of the BNBT 5.5 and BNBT 8.0 thin films and powders.

In the case of the BNBT5.5 and BNBT8.0 films, broad peaks, which are fitted considering the coexistence of rhombohedral and tetragonal structures, are observed for the full 2θ diagrams, using tilt angles from χ=25º to 55º(insets of figure 4 and 5). From the patterns obtained with χ=0º to 20º, the large intensity of the peaks around 2θ~40º and ~47º reveals the contribution of the reflections attributed to the (111) and (200) of the Pt-electrode of the substrate, respectively. However, for higher χ angles no change in the intensity of the reflections is observed. These reflections would be only

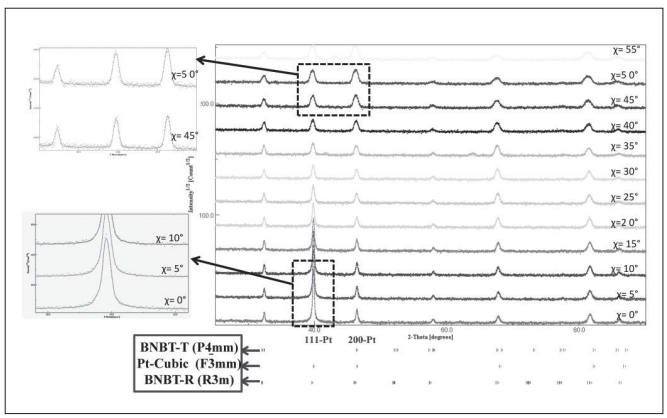

Figure 4. Experimental X-ray diagrams for BNBT5.5 thin film and their corresponding fitted recorded for tilted angles from χ= 0° to 55°, azimuthal angle of ϕ=20 ° and in the 2θ interval from 0° to 120°. Insets show the experimental XRD pattern (dotted line) and the calculated profile (solid line).

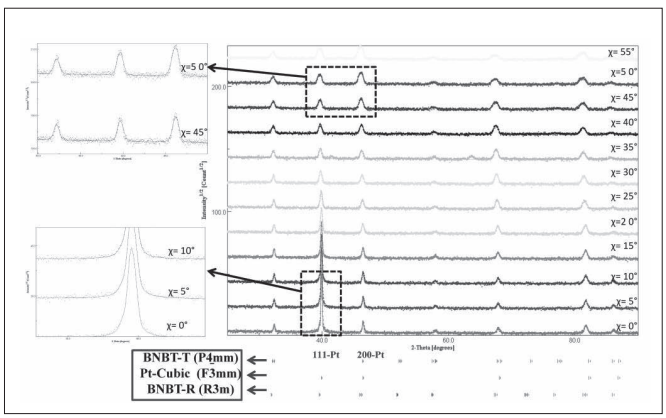

Figure 5. Experimental X-ray diagrams for BNBT8.0 thin film and their corresponding fitted recorded for tilted angles from χ= 0° to 55°, azimuthal angle of ϕ=20 ° and in the 2θ interval from 0° to 120°. Insets show the experimental XRD pattern (dotted line) and the calculated profile (solid line).

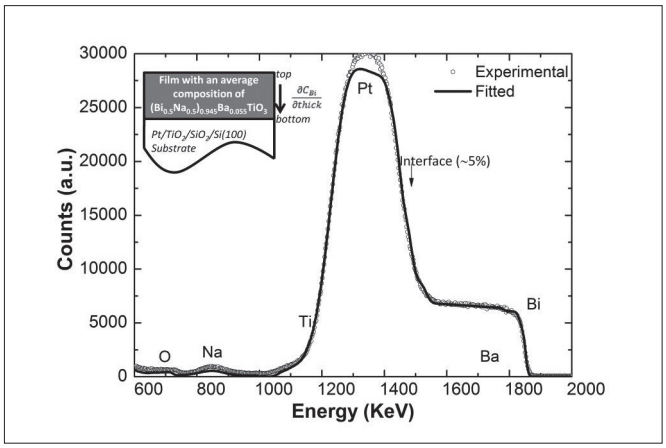

Figure 6. Compositional depth profile of the BNBT5.5 thin film deposited onto $Pt/TiO_2/SiO_2/Si(100)$ substrate measured by RBS, using a 2 Mev He^+ beam and a barrier detector at $\theta = 170^o$. Inset show the schematic cross sectional representation of the film inferred from the simulation.

associated with the perovskite, therefore indicating that the films are not textured.

These results clearly indicate for these BNBT polycrystalline thin films and their corresponding powders a progressive change from the rhombohedral to the tetragonal symmetry as a function of the Ba^{2+} content for a composition range around x ~ 0.055-0.080, where both structures coexist. This is characteristic of a MPB region. In addition, it has to be noted that the special conditions of processing of the films (rapid thermal treatment with a rapid heating rate of ~303 $K \cdot s^{-1}$ and oxygen atmosphere) hinder the formation of the secondary phases observed in the corresponding powders processed in a conventional oven.

According to the RBS spectra, homogenous compositional depth profiles have been obtained for the BNBT films. Representative experimental and calculated profiles are shown in Figure 6 for the BNBT5.5 film (25, 26). For the calculation of the bulk film thickness, the theoretical density of the $(Bi_{0.5}Na_{0.5})TiO_3$ perovskite (5.92g cm^{-3}) has been considered. A good agreement is obtained for a ~325 nm thick film with

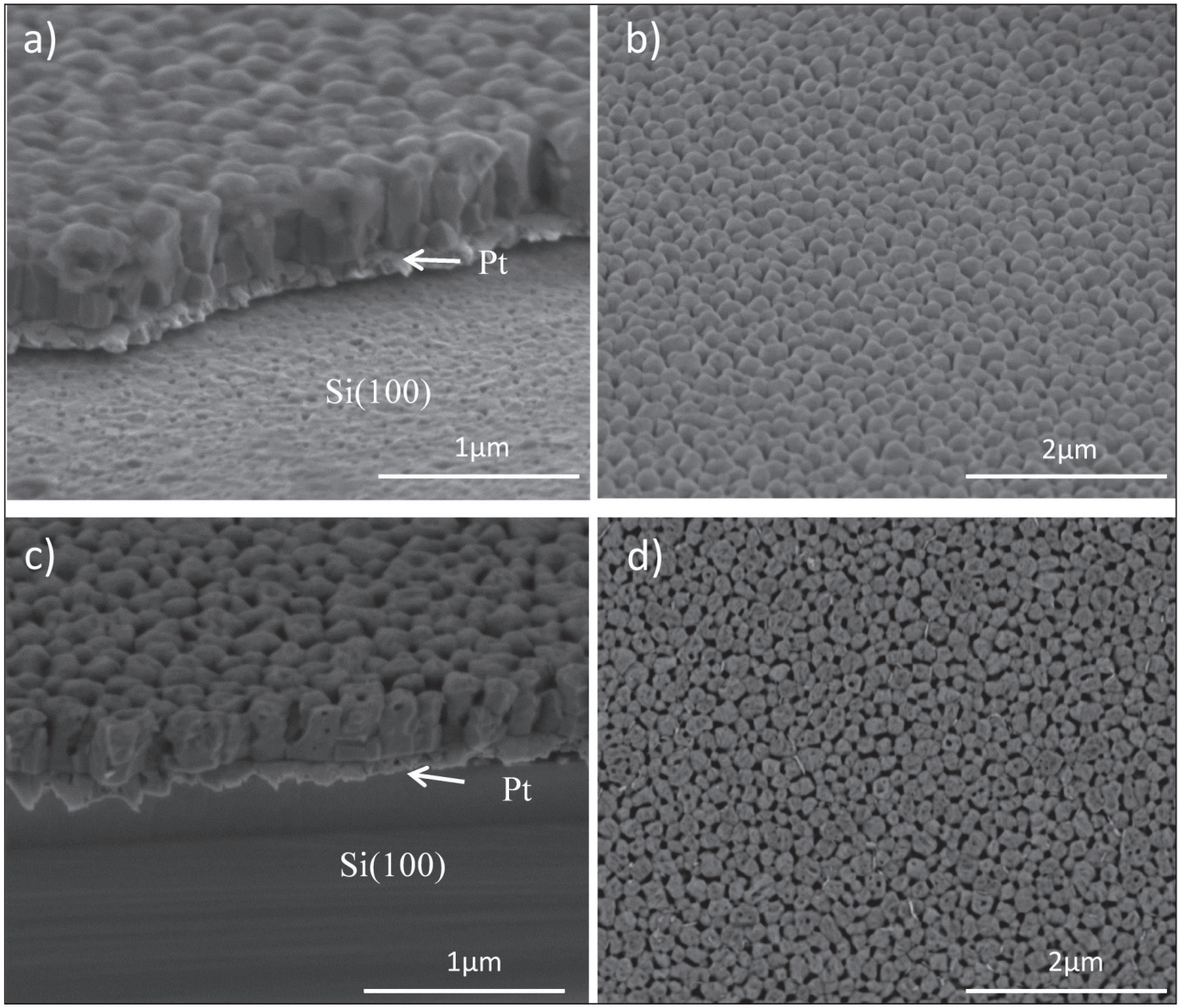

Figure 7. Cross-section and plan-view FEGSEM micrographs of the a),b) BNBT5.5 thin film and c), d) BNBT8.0 thin film.

a $(Bi_{0.5}Na_{0.5})_{0.945}Ba_{0.055}TiO_3$ composition and an abrupt interface between the film and the substrate. This thin interface is ascribed to a Bi_xPt layer, consequence of the reaction between the Bi from the film and the Pt from the bottom electrode of the substrate (27).The thickness of this interface is estimated to be of a ~5 % of the total thickness which is close to the resolution limit of the technique. The content of Na^+ could not be determined by RBS due to the low atomic number of this element. Besides, the energy of the backscattered ions associated with Na overlaps those of Ti and O elements.

The microstructures of the BNBT5.5 and BNBT8.0 thin films have been investigated by Scanning Electron Microscopy (Figure 7). Thicknesses of ~ 340 nm and ~ 280 nm have been calculated from these micrographs for the BNBT5.5 and BNBT8.0 films, respectively. These thickness values are of the same order as those obtained by RBS, which is indicative of the formation of single perovskite films with the nominal composition and without secondary phases, porosity or thick interfaces.

4. CONCLUSIONS

For the solution-derived $(Bi_{0.5}Na_{0.5})_{1-x}Ba_xTiO_3$ (BNBT) thin films of this work, the crystalline structure could be tailored with the Ba^{2+}content of the solid solution. An evolution from the rhombohedral to the tetragonal structure with the increase of the Ba^{2+} content is observed in these BNBT films.

The MPB region for the BNBT thin films is located for x~0.055-0.080, where X-ray diffraction data have been fitted considering the coexistence of a tetragonal and a rhombohedral phase. These results support recent structural studies carried out in BNBT bulk ceramics as well as data here included for powders.

These BNBT thin films processed by CSD and crystallized by RTP treatments have homogeneous microstructures and compositional depth profiles without appreciable film/substrate interfaces. This joined to the coexistence of rhombohedral and tetragonal crystalline structures in the MPB region for x~0.055-0.080 make possible to predict in these MPB-BNBT films appropriate functional properties of interest for applications.

ACKNOWLEDGEMENTS

This work was financed by Spanish Project MAT2010-15365. D. Pérez-Mezcua is grateful for the financial support of the FPU Spanish program. Dr I. Bretos acknowledges for the financial support of the Juan de la Cierva Spanish program. Dr R. Escobar- Galindo acknowledges support through Ramon y Cajal program (RyC2007-0026).

REFERENCES

1. P. Muralt. Ferroelectric thin films for micro-sensors and actuators: a review. *J. Micromech. Microeng*. 10, 136–146 (2000)
2. M. Ahart, M. Somayazulu, R. E. Cohen, P. Ganesh, P. Dera, H. Mao,R. J. Hemley, Yang Ren, P. Liermann, Z. Wu. Origin of morphotropic phase boundaries in ferroelectrics. *Nature*. 451, 545-549, (2008)
3. J. Rödel, W. Jo, K. T. P. Seifert, E. Anton, T. Granzow. Perspective on the Development of Lead-free Piezoceramics. *J. Am. Ceram. Soc.* 92 [6], 1153–1177, (2009)
4. V. A. Isupov. Ferroelectric $Na_{0.5}Bi_{0.5}TiO_3$ and $K_{0.5}Bi_{0.5}TiO_3$Perovskite and their Solid Solutions. *Ferroelectrics*, 315, 123-147, (2005)
5. G. O. Jones, P. A. Thomas. Investigation of the structure and phase transitions in the novel A-site subtituted distorted perovskite compound $Na_{0.5}Bi_{0.5}TiO_3$. *Acta Crystallogr*. B. B58, 168-78, (2002)
6. W. Ji , Y. Chen, S. Zhang, B. Yang, X. Zhao, Q. Wang. Microstructure and electric properties of lead-free $0.8Bi_{1/2}Na_{1/2}TiO_3$–$0.2Bi_{1/2}K_{1/2}TiO_3$ceramics. *Ceram. Int.* 38, 1683–1686, 2012
7. V. Dorcet, P. Marchet, G. Trolliard. Structural and dielectric studies of the $Na_{0.5}Bi_{0.5}TiO_3$- $BiFeO_3$ system. *J. Eur. Ceram. Soc.* 27, 4371-74, (2007)
8. C. Xu, D. Lin, K. W. Kwok. Structure, electrical properties and depoling temperature of $Bi_{1/2}Na_{1/2}TiO_3$-$BaTiO_3$ lead- free piezoelectric ceramics. *Solid State Sci.* 10, 934-40, (2008)
9. J. Trelcat, C. Courtois, M. Rguiti, A. Leriche, P. Duvigneaud, T. Segato. Morphotropic phase boundary in the BNT–BT–BKT system. *Ceram. Int*. 38, 2823–2827, (2012)
10. C. Zhou, X. Liu,W. Li, C. Yuan. Structure and piezoelectric properties of $Bi_{1/2}Na_{1/2}TiO_3$–$Bi_{1/2}K_{1/2}TiO_3$ –$BiFeO_3$ lead-free piezoelectric ceramics. *Mater. Chem. Phys.* 114 832–836, (2009)
11. T. Takenaka, K. Sakata. Dielectric, Piezoelectric and Pyroelectric properties of $(Na,Bi)_{1/2}TiO_3$- Based Ceramics. *Ferroelectrics.* 95, 153-6, (1989)
12. D. Rout, K. S. Moon, S. Rao, S. J. Kang. Study of the morphotropic phase boundary in the lead-free $Na_{1/2}Bi_{1/2}TiO_3$-$BaTiO_3$ system by Raman spectroscopy. *J. Ceram. Soc. Jpn*. 117, 797-800, (2009)
13. P. A. Thomas, S. Trujillo, M. Bourdard, S. Gorfman , J. Kreisel. Diffuse X- ray scattering in the lead- free piezoelectric crystals $Na_{1/2}Bi_{1/2}TiO_3$ and Ba- doped $Ba_{1/2}Bi_{1/2}TiO_3$. *Solid State Sci.* 12, 311-17, (2010)
14. T. Takenaka, K. Maruyama, K. Sakata. $Na_{1/2}Bi_{1/2}TiO_3$-$BaTiO_3$ system for lead-free piezoelectric ceramics. *Jpn. J. Appl. Phys.* 30, 2236-2239, (1991)
15. W. Jo, J. Rödel. Electric-field-induced volume change and room temperature phase stability of $(Bi_{1/2}Na_{1/2})TiO_3$-x mol. % $BaTiO_3$piezoceramics. *Appl. Phys. Lett*. 99, 042901, (2011)
16. N. Setter, D. Damjanovic, L. Eng, G. Fox, S. Gevorgian, S. Hong, A. Kingon, H. Kohlstedt, N. Y. Park, G. B. Stephenson, I. Stolitchnov, A. K. Taganstev, D. V. Taylor, T. Yamada and S. Streiffer. Ferroelectric thin films: Review of materials, properties, and applications. *J. Appl. Phys.* 100, 051606, (2006)
17. H. W. Cheng, X. J. Zhang, S. T. Zhang, Y. Feng, Y. F. Chen. Combinatorial studies of (1-x) $Na_{0.5}Bi_{0.5}TiO_3$-$XBaTiO_3$ thin- film chips. *Appl. Phys. Lett*. 85, 2319-21, (2004)
18. I. Bretos, D. Alonso- San José, R. Jiménez, J. Ricote, M. L. Calzada .Evidence of morphotropic phase boundary displacement in lead- free $(Na_{0.5}Bi_{0.5})_{1-x}Ba_xTiO_3$ polycrystalline thin films.*Mater.Lett*. 65, 2714-16, (2011)
19. C. Dragoi, M. Cernea, L. Trupina. Lead- free ferroelectric $BaTiO_3$ doped-$Na_{0.5}Bi_{0.5}TiO_3$ thin films processed by pulsed laser deposition technique. *Appl. Surf. Sci*., 257, 9600-05, (2011)
20. R. W. Schwartz, T. Schneller , R. Waser. Chemical solution deposition of electronic oxide films.*C. R. Chimie*. 7, 433–461, (2004)
21. D. Alonso- Sanjosé, R. Jiménez, I. Bretos, M. L. Calzada. Lead- free $Bi_{1/2}Na_{1/2}TiO_3$-$BaTiO_3$ ferroelectric thin films in the morphotropic phase boundary composition: solution processing and properties. *J. Am. Ceram. Soc.* 92[10], 2218-25, (2009)
22. S. Hoffmann, R. Waser. Control of the Morphology of CSD- prepared (Ba, Sr)TiO_3 thin films. *J. Eur. Ceram. Soc.* 19, 339-43, (1999)
23. W. Jo, J. E. Daniel, J. L. Jones, X. Tan, P. A. Thomas, D. Damjanovic, J. Rödel .Evolving morphotropic phase boundary of $Bi_{1/2}Na_{1/2}TiO_3$-$BaTiO_3$ piezoceramics. *J. Appl. Phys*. 109, 014110, (2011)
24. L. Lutterotti. Materials Analysis Using Diffraction. http://www.ing.unitn.it/~maud/
25. E. Kotai. Computer method for analysis and simulation of RBS and ERDA spectra. *Nucl. Instrum. Methods. B.* 85, 588–96, (1994)
26. M. Mayer. SIMNRA: Simulation of RBS, ERD and NRA spectra. http://www.rzg.mpg.de/_mam/
27. M. L. Calzada, R. Jiménez, A. González, J. García-López, D. Leinen, E. Rodríguez-Castellón. Interfacial effects and electrical characteristics of ferroelectric strontium bismuth tantalate thin films on Pt/TiO_2 and Ti/Pt/Ti heterostructure electrodes. *Chem. Mater*. 17, 1441-1449, (2005)

Recibido: 20/06/2013
Recibida versión corregida: 16/12/2013
Aceptado: 17/12/2013